Quasi-elastic scattering, random fields and phonon-coupling effects in $PbMg_{1/3}Nb_{2/3}O_3$

2005 J. Phys.: Condens. Matter 17 4343

(http://iopscience.iop.org/0953-8984/17/27/010)

INSTITUTE OF PHYSICS PUBLISHING JOURNAL OF PHYSICS: CONDENSED MATTER

J. Phys.: Condens. Matter **17** (2005) 4343–4359 doi:10.1088/0953-8984/17/27/010

Quasi-elastic scattering, random fields and phonon-coupling effects in $PbMg_{1/3}Nb_{2/3}O_3$

S N Gvasaliya[1,3,4], B Roessli[1], R A Cowley[2], P Huber[1] and S G Lushnikov[3]

[1] Laboratory for Neutron Scattering ETHZ and Paul Scherrer Institut, CH-5232 Villigen PSI, Switzerland
[2] Clarendon Laboratory, Oxford University, Parks Road, Oxford OX1 3PU, UK
[3] Ioffe Physical Technical Institute, 26 Politekhnicheskaya, 194021, St Petersburg, Russia

E-mail: severian.gvasaliya@psi.ch

Received 24 May 2005, in final form 9 June 2005
Published 24 June 2005
Online at stacks.iop.org/JPhysCM/17/4343

Abstract

The low energy part of the vibration spectrum in $PbMg_{1/3}Nb_{2/3}O_3$ (PMN) relaxor ferroelectric has been studied by means of neutron scattering above and below the Burns temperature, T_d. The transverse acoustic and the lowest transverse optic phonons are strongly coupled and we have obtained a model for this coupling. We observe that the lowest optic branch is always underdamped. A resolution-limited central peak and quasi-elastic scattering appear in the vicinity of the Burns temperature. It is shown that it is unlikely that the quasi-elastic scattering originates from the combined effects of coupling between TA and TO phonons with an increase of the damping of the TO phonon below T_d. The quasi-elastic scattering has a peak as a function of temperature close to the peak in the dielectric constant while the intensity of the central peak scattering increases strongly below this temperature. These results are discussed in terms of a random field model for relaxors.

(Some figures in this article are in colour only in the electronic version)

1. Introduction

The family of complex perovskites $AB'_xB''_{1-x}O_3$ has been known for fifty years and they are related to the classic ABO_3 perovskites but with different physical properties due to the chemical disorder on the B sublattice. A very interesting subclass of these complex perovskites is formed by the relaxor ferroelectrics, or briefly—relaxors. These materials have a frequency dependent peak in the dielectric permittivity ε' which typically extends over hundreds of degrees and is not directly related to any macroscopic changes of the symmetry. Since many physical properties of relaxors exhibit anomalies in this temperature range, the properties were

[4] Author to whom any correspondence should be addressed.

called a 'diffuse phase transition'. Despite many investigations, however, the nature of the diffuse phase transition remains unclear [1–5].

$PbMg_{1/3}Nb_{2/3}O_3$ (PMN) is a model relaxor ferroelectric. It has the cubic $Pm\bar{3}m$ structure at all temperatures in the absence of an external electric field [6]. However, in an applied electric field, PMN undergoes a structural phase transition at $T \sim 210$ K [7] while the anomaly in the dielectric permittivity ε' appears around the mean Curie temperature $T_{cm} \sim 270$ K [1]. At a higher temperature, $T_d \sim 620$ K, the optical refractive index departs from the expected linear temperature dependence as observed by Burns and Scott [8]. This result was explained by the appearance of small polar regions of the size of a few unit cells, which were referred to as 'polar nanoregions' (PNR).

The lattice dynamics of PMN and similar relaxor crystals $PbMg_{1/3}Ta_{2/3}O_3$ (PMT), $PbZn_{1/3}Nb_{2/3}O_3$ (PZN) and $PbZn_{1/3}Nb_{2/3}O_3$–$x$$PbTiO_3$ (PZN–xPT) has been studied by means of light [8–13] and neutron scattering [14–28, 30]. First-order Raman light scattering was observed in both PMN and PZN [8], although first-order scattering is forbidden if the crystal structure remains that of the cubic perovskites. Until now there has been no detailed understanding of the origin of the apparent first-order Raman scattering in the relaxors [12, 13]. The search for a soft mode by means of light scattering in PMN was unsuccessful [8, 12], whereas the results of neutron scattering measurements have led to the suggestion that the soft TO phonons are overdamped for $q \lesssim 0.12$ rlu and 200 K $\lesssim T \lesssim T_d$ [16, 19, 21]. This anomalous behaviour of the TO phonons was attributed to the formation of PNR in both PZN and PMN [17–19, 21], although an alternative interpretation was recently proposed that describes the results and the so-called 'waterfall' effect in terms of coupling between TA and highly damped TO phonons [24]. In addition, both light and neutron spectroscopy have reported a quasi-elastic (QE) component in the phonon spectrum of PMN [9, 11, 13, 27, 28, 30]. As anharmonicity is important in relaxors, it is *a priori* possible that this quasi-elastic mode originates from the strong coupling between the TA and heavily damped TO phonon modes [32].

In this work we have used high resolution neutron scattering to investigate the low energy part of the vibration spectrum of PMN as described in section 2. We find in section 3 that the lowest transverse optical (TO) phonon branch is strongly coupled to the transverse acoustic branch (TA) above the Burns temperature, T_d, where the QE component is absent. Below T_d, the results suggest that the phonon spectrum remains essentially unchanged, with the TO phonons found to be underdamped throughout the temperature range, and the 'waterfall effect' is not clearly observed at least in the $[0, 0, q]$ direction. In addition there are two more components of the scattering consisting of a quasi-elastic, QE, component whose energy width is larger than the resolution and a central peak, CP, component whose energy width is the same as the resolution function. The energy and wavevector width of the QE component have been measured and it is found that the QE susceptibility is a maximum at a temperature of about 370 K, a somewhat larger temperature than the maximum in the dielectric susceptibility. The CP component increases rapidly in intensity below 370 K similarly to the behaviour expected from an order parameter. The line shape of the scattering as a function of wavevector is not however a sharp Bragg reflection but is approximately a Lorentzian to the power of 1.5. In section 4 we shall suggest that these results are consistent with a random field model for this relaxor.

2. Experimental details

The measurements were carried out with the three-axis spectrometer TASP, located at the neutron spallation source SINQ at the Paul Scherrer Institut, Switzerland. A high quality

single crystal of PMN ($\sim$8 cm^3) was mounted using a niobium holder inside a furnace. The measurements were performed in the temperature range 150–670 K. The crystal was aligned in the (*hhl*) scattering plane. The spectrometer had a pyrolytic graphite (PG) monochromator and analyser and was operated in the constant-final-energy mode. In the course of the measurements we had to search for compromises between the spectrometer resolution, the accessible (Q–ω) range and the intensity. As a result several different spectrometer configurations were used. Most of data were collected in the following three configurations:

(i) $k_f = 1.64$ Å^{-1} and 10′/Å–80′–80′–80′ collimation,
(ii) $k_f = 2.662$ Å^{-1} and 10′/Å–80′–80′–80′ collimation,
(iii) $k_f = 2.662$ Å^{-1} and 10′/Å–20′–20′–80′ collimation,

where k_f refers to the energy of the scattered neutrons. In configuration (i) the (002) Bragg reflection of PG was used for both the monochromator and analyser, whereas the (004) reflection was used for configurations (ii) and (iii). The energy resolution at zero energy transfer was 0.22 meV for configuration (i), 0.5 meV for (ii) and 0.25 meV for (iii). For configuration (i) the q-resolution along the scattering vector was $q_{\rm par} = 0.015$ Å^{-1} and $q_{\rm perp} = 0.021$ Å^{-1} in the transverse direction. For configurations (ii) and (iii) $q_{\rm par} = 0.02$ Å^{-1} and $q_{\rm perp} = 0.04$ Å^{-1}, respectively. The vertical resolution was $q_z = 0.1$ Å^{-1} with $k_f = 1.64$ Å^{-1} and $q_z = 0.16$ Å^{-1} with $k_f = 2.662$ Å^{-1}, respectively.

3. Experimental results and data analysis

3.1. Measurements above the Burns temperature at $T = 670$ K

The dynamical susceptibility for two coupled excitations was considered, for example in [31–33], and is given by

$$\chi_{\rm CM}(\mathbf{Q},\omega) = \frac{f_1^2\chi_1 + f_2^2\chi_2 + 2\lambda f_1 f_2 \chi_1\chi_2}{1-\lambda^2\chi_1\chi_2}, \tag{1}$$

where $\chi_i \equiv \chi_i(\mathbf{Q},\omega)$, $i = 1, 2$, are the dynamical susceptibilities of the uncoupled phonons; and the f_i are the wavevector dependent structure factors for the modes. The interaction term contains both real and imaginary parts and is assumed to have the simplified form: $\lambda \equiv \Delta + {\rm i}\Gamma_{12} = (\Delta_{12} + {\rm i}\omega\gamma_{12})\sin^2(\pi q)$ where the q dependence is chosen to be proportional to q^2 at small q as expected for a centrosymmetric crystal [31]. The dynamical susceptibilities of the TA and TO phonons are given by the damped harmonic oscillator functions (DHO):

$$\chi_{\rm DHO}(\mathbf{q},\omega) = (\omega_{\mathbf{q}}^2 - {\rm i}\gamma_{\mathbf{q}}\omega - \omega^2)^{-1}. \tag{2}$$

In equation (2), γ_q is the damping and ω_q is the renormalized frequency of a phonon.

When the damping is neglected the resonance frequency of the two coupled modes is given by

$$\Omega_{1,2}^2 = \tfrac{1}{2}\left(\omega_1^2 + \omega_2^2 \pm \sqrt{(\omega_1^2-\omega_2^2)^2 + 4\Delta}\right), \tag{3}$$

where ω_1 and ω_2 are the frequencies of uncoupled excitations. To model the dispersion of the TA and TO phonons we have used the following parameterization based on a low q expansion:

$$\omega_1 \equiv \omega_{\rm TA} = d\sin(\pi q), \tag{4}$$

and

$$\omega_2^2 \equiv \omega_{\rm TO}^2 = \omega_{\rm TO}^2(0) + c\sin^2(\pi q). \tag{5}$$

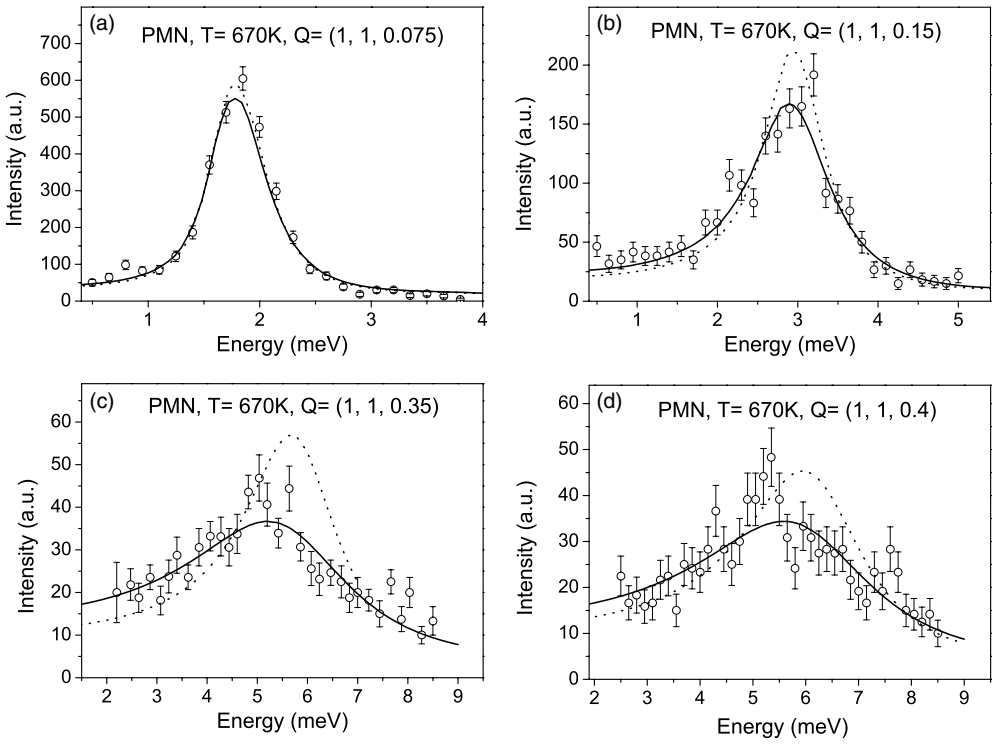

Figure 1. The results of typical constant-Q scans using configuration (i) in the (1, 1, 0) BZ. The solid line shows the fit results whereas the dotted line corresponds to simulated spectra with the imaginary part of the coupling set to zero. See the text for details. q is given in reciprocal lattice units (rlu). 1 rlu = 1.55 Å^{-1}.

The damping of TA phonon was found to increase with q approximately as

$$\gamma_{\mathrm{TA}} = D_{\mathrm{TA}} \sin^2(\pi q) \tag{6}$$

and no assumption was made about the damping of the TO phonon.

The neutron scattering intensity $I(\mathbf{Q}, \omega)$ was modelled as

$$I(\mathbf{Q}, \omega) = S(\mathbf{Q}, \omega) \otimes R(\mathbf{Q}, \omega) + B. \tag{7}$$

The symbol $\otimes$ stands for the 4D convolution with the spectrometer resolution function $R(\mathbf{Q}, \omega)$ [34], while B denotes the background level and $S(\mathbf{Q}, \omega)$ is the neutron scattering function which is related to the imaginary part of the dynamical susceptibility, $\chi''(\mathbf{Q}, \omega)$, through

$$S(\mathbf{Q}, \omega) = \frac{[n(\omega) + 1]}{\pi} \chi''_{\mathrm{CM}}(\mathbf{Q}, \omega) \tag{8}$$

with the temperature factor $[n(\omega) + 1] = [1 - \exp(-\hbar\omega / k_{\mathrm{B}} T)]^{-1}$.

Figures 1 and 2 show typical inelastic neutron scattering spectra of PMN at $T = 670$ K in the (1, 1, 0) and (2, 2, 0) Brillouin zones (BZ) and the results of fitting these spectra to the interacting phonon model, equation (8). In the (1, 1, 0) BZ only the TA phonon is observed in constant-Q scans, whereas both TA and TO phonons are visible in the (2, 2, 0) BZ. The values of parameters which correspond to the solid lines in figures 1 and 2 are: $d = 10.05 \pm 0.45$ meV, $D_{\mathrm{TA}} = 4.1 \pm 0.5$ meV, $\omega_{\mathrm{TO}}(0) = 2.1 \pm 0.2$ meV, $c = 137 \pm 9$ meV^2, $\Delta_{12} = 85 \pm 7$ meV^2,

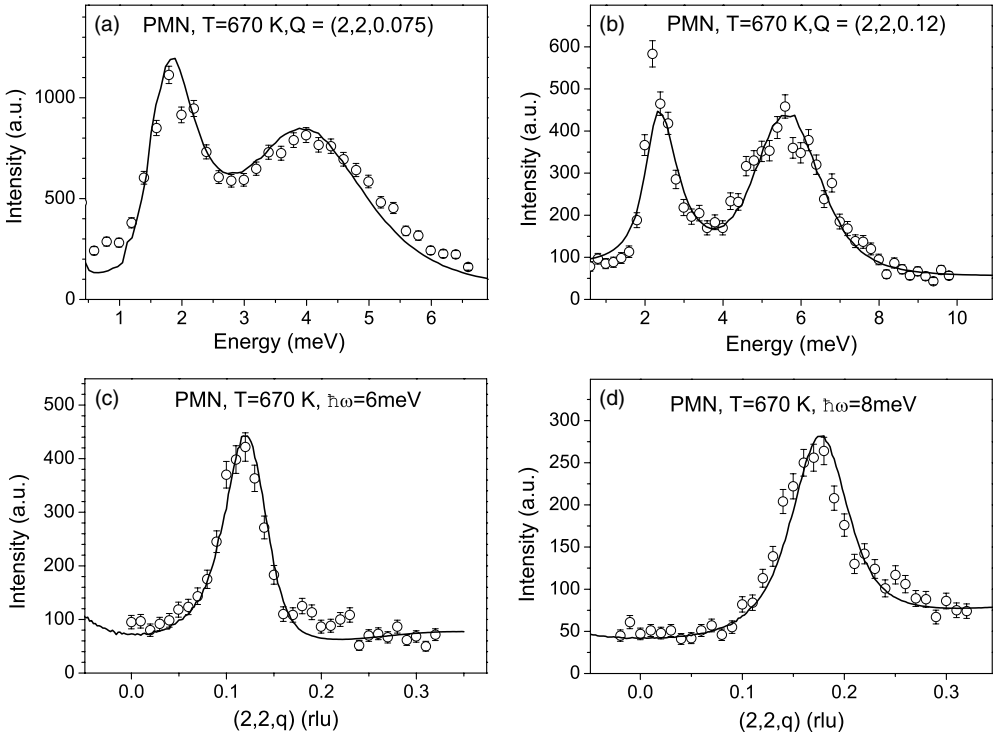

Figure 2. The results of typical constant-Q and the results of constant-E scans taken in the (2, 2, 0) BZ using configuration (ii) with results of fits as explained in the text.

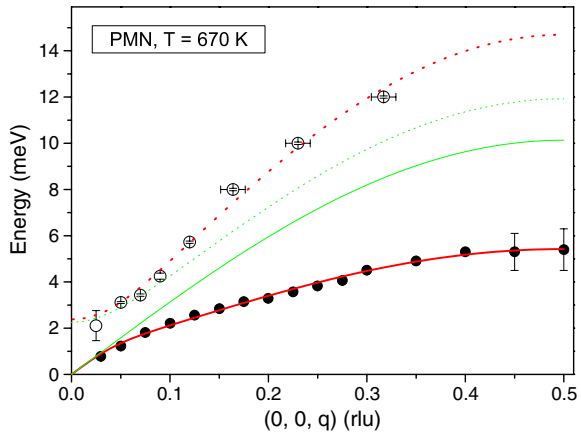

Figure 3. Observed and calculated dispersion of the TA (solid circles) and the lowest TO (open circles) phonons in PMN along the [0, 0, q] direction measured at $T = 670$ K. The solid and dotted green lines correspond to the calculated dispersion of the TA and TO phonons with the coupling set to zero.

$\gamma_{12} = 1.5 \pm 0.5$ meV. The wavevector dependence of the damping of the TO phonon, γ_{TO}, is given in table 1. The TA and TO dispersion curves are correctly reproduced with this parameterization and the frequencies are shown in figure 3. Also shown in figure 3 is the

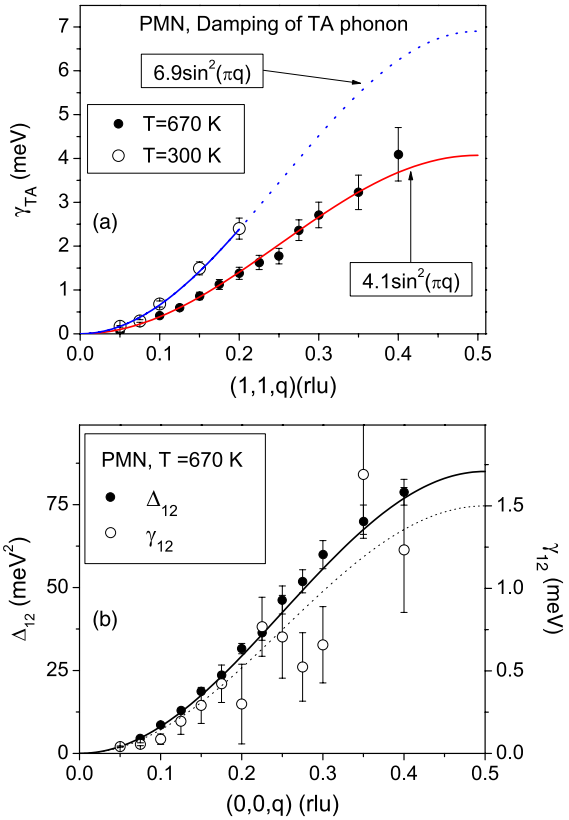

Figure 4. (a) q dependence of the damping of the transverse acoustic phonon $T = 670$ and 300 K. (b) q dependence of the real and imaginary parts of the coupling (see the text for details).

dispersion of the TA and TO branches in the absence of coupling. The two branches do not cross and the dispersion of both branches is mostly affected by the coupling close to the zone boundary. As illustrated in figure 1 the imaginary part of the coupling affects the phonon line shape mainly at large momentum transfers. Figure 4 shows that the dampings of the TA phonon and the coupling term are proportional to $\sin^2(\pi q)$, as obtained from fitting the spectra individually. Finally, figure 5 shows the structure factor of the TA and TO modes.

3.2. Temperature dependence of the vibration spectrum

The energy and q space resolution was improved to study the temperature dependence of the TA and TO modes close to the Brillouin zone centre. Figures 6 and 7 show examples of spectra measured at $\mathbf{Q} = (2, 2, 0.05)$ and $\mathbf{Q} = (1, 1, 0.05)$, respectively. At 670 K, apart from the resolution-limited elastic scattering, only scattering from the TA and TO phonons is observed. Upon decreasing the temperature, additional quasi-elastic scattering, QE, becomes visible with an energy width larger than the resolution function, while the more intense strictly elastic scattering, the CP component, increases on cooling especially below a temperature of 370 K. Both components of this elastic scattering have been observed previously in PMN [27, 28] and can be described by a resolution-limited central peak (CP) and a Debye-like relaxation mode.

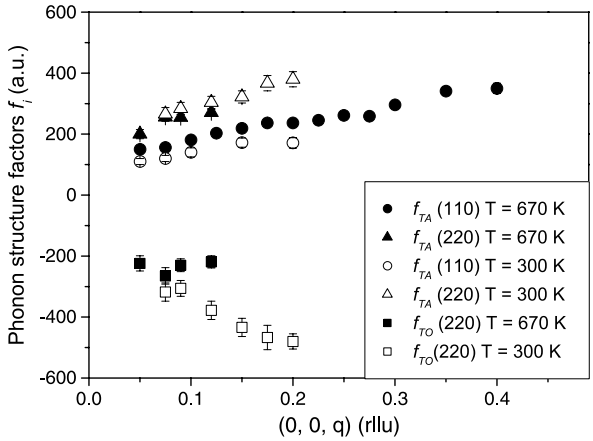

Figure 5. Wavevector dependence of the structure factors of the TA and TO phonons along the $[0, 0, q]$ direction.

Table 1. (a) Wavevector dependence of γ_{TO} and (b) temperature dependence of the frequency and of the damping of the TO phonon at $q = 0.05$ rlu in PMN.

(a)							
q (rlu)	0.05	0.075	0.09	0.12	0.15	0.175	0.2
γ_{TO}(670 K) (meV)	0.8	1.4	1.8	1.3	—	—	—
Std error	0.1	0.2	0.3	0.2	—	—	—
γ_{TO}(300 K) (meV)	1.0	1.8	2.0	2.4	3.9	4.2	4.4
Std error	0.2	0.3	0.4	0.4	0.7	0.9	0.9

(b)					
T (K)	670	595	502	410	300
ω_{TO} (0.05 rlu) (meV)	2.69	2.68	2.69	2.71	2.70
Std error	0.02	0.03	0.02	0.02	0.02
γ_{TO} (0.05 rlu) (meV)	0.8	0.9	0.8	0.9	1.0
Std error	0.1	0.1	0.1	0.1	0.2

The neutron scattering susceptibility is given by

$$S(\mathbf{Q}, \omega) = S_{CP}(\mathbf{Q}, \omega) + \frac{[n(\omega) + 1]}{\pi}[\chi''_{CM}(\mathbf{Q}, \omega) + f^2_{QE}(\mathbf{Q})\chi''_{QE}(\mathbf{Q}, \omega)], \quad (9)$$

$$S_{CP} = A(\mathbf{Q})\delta(\omega), \quad (10)$$

$$\chi_{QE}(\mathbf{q}, \omega) = \frac{\chi(0, T)}{1 + q^2\xi^2}(1 - i\omega/\Gamma_q)^{-1}, \quad (11)$$

where $\delta(\omega)$ is the Dirac function; f_{QE} is the structure factor of the QE component and $\chi(0, T)$ is the susceptibility at $q = 0$; ξ is the correlation length of the QE scattering and $\Gamma_q = \Gamma_0 + D_{QE}q^2$. S_{CP} describes the resolution-limited central peak with intensity $A(\mathbf{Q})$.

The model, described by equations (7)–(11), was fitted to the neutron scattering at various temperatures and it gave good agreement with the results provided that the elastic scattering components were included. Typical results are shown in figures 6 and 7. In the temperature range between 300 and 670 K for $q = 0.05$ rlu, the parameters describing the phonon line shape remain essentially unchanged for this small wavevector (see table 1). However, the damping and the amplitude of the QE scattering change significantly as will be discussed in the next subsection.

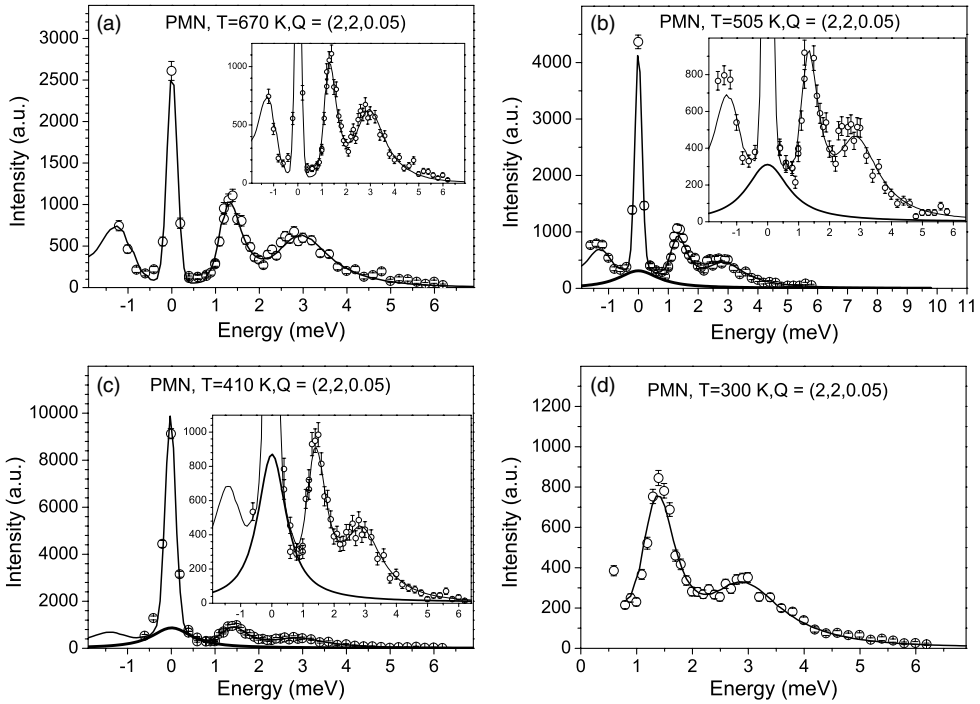

Figure 6. Observed and calculated spectra from constant-Q scans taken at $\mathbf{Q} = (2, 2, 0.05)$ as a function of temperature. The contribution of QE scattering is shown by a bold solid line.

A more detailed measurement of the scattering as a function of wavevector was performed with constant-Q scans around both the (1, 1, 0) and (2, 2, 0) BZ at $T = 300$ K. The results for the scattering and the fits to the model are shown in figures 8 and 9. We observe an increase of the damping of the TA and TO phonons and of the stiffness of the TO branch. The values of the TA damping and TO stiffness at $T = 300$ K are $D_{\mathrm{TA}} = 6.9 \pm 0.6$ meV and $c = 260 \pm 25$ meV^2; the momentum dependence of the TO phonon damping is summarized in table 1. It is clear from the spectra shown in figure 9 and from table 1 that at $T = 300$ K the lowest TO phonon is underdamped over the entire range of wavevectors. Also the structure factors of the acoustic and optical branches do not change significantly with temperature as shown in figure 5.

The conclusion from this fitting is that although there is some temperature dependence of the phonon spectra at large wavevectors q, at small wavevectors there is little temperature dependence and we can essentially consider the low q, high energy phonons as temperature independent.

The constant-energy scans in PMN along $[2, 2, q]$ were measured to investigate the 'waterfall effect' for $\hbar\omega = 4$, 6 and 8 meV. The solid lines in figure 10 were obtained by varying only the intensities of the phonons and of the QE scattering while the other parameters of the phonons were fixed at the values obtained for $T = 300$ K. The model fits the experimental data very satisfactorily. We observe that the maxima in the spectra vary with the energy showing that the 'waterfall' is not present at $T = 500$ K at least in the (2, 2, 0) Brillouin zone.

3.3. Temperature dependence of the elastic scattering

The temperature dependences of the two components of the elastic scattering were also obtained from the fits of the model. Initially we shall consider the quasi-elastic scattering. The intensity

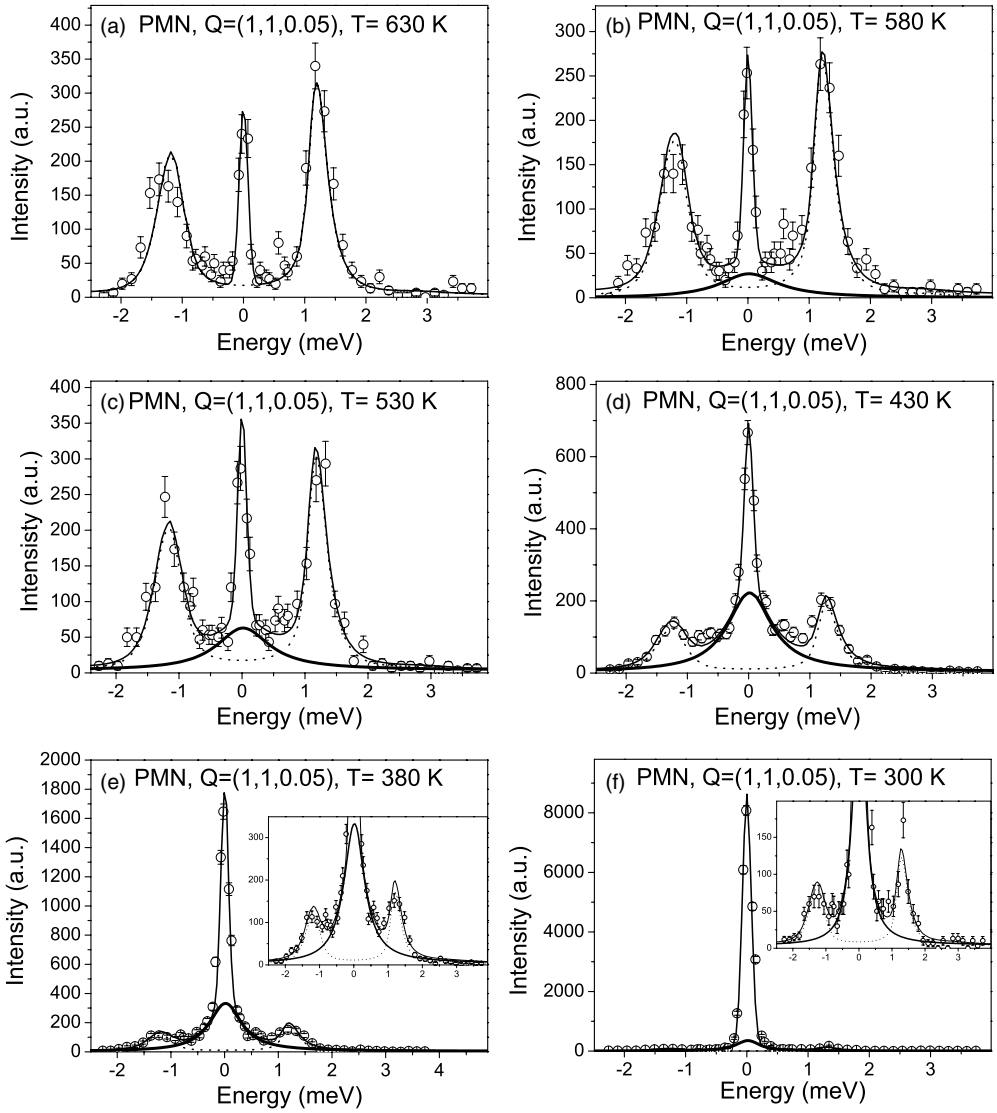

Figure 7. Observed and calculated spectra from constant-Q scans taken at $\mathbf{Q} = (1, 1, 0.05)$. The contribution of QE scattering is shown by a bold solid line. Note the increase of CP intensity as the temperature is lowered below T_d. These measurements were performed using $k_f = 1.64$ Å^{-1} and $10'/\text{Å}-20'-20'-80'$ collimation.

of the quasi-elastic scattering is shown in figure 11. It increases on cooling below 600 K reaching a maximum at about 370 K and then decreases on further cooling. The frequency width of the scattering is shown in figure 12 as deduced from measurements with $q = 0.05$ rlu. Γ decreases with decreasing temperature from about 0.5 meV at 600 K to 0.1 meV at 200 K. The wavevector dependence of the width has been studied at temperatures of 450 and 300 K and is shown in figure 13 for the latter temperature. It increases with wavevector q and is at least approximately proportional to a constant and a quadratic term, as suggested above by equation (11). The wavevector dependence of the energy-integrated intensity of the quasi-

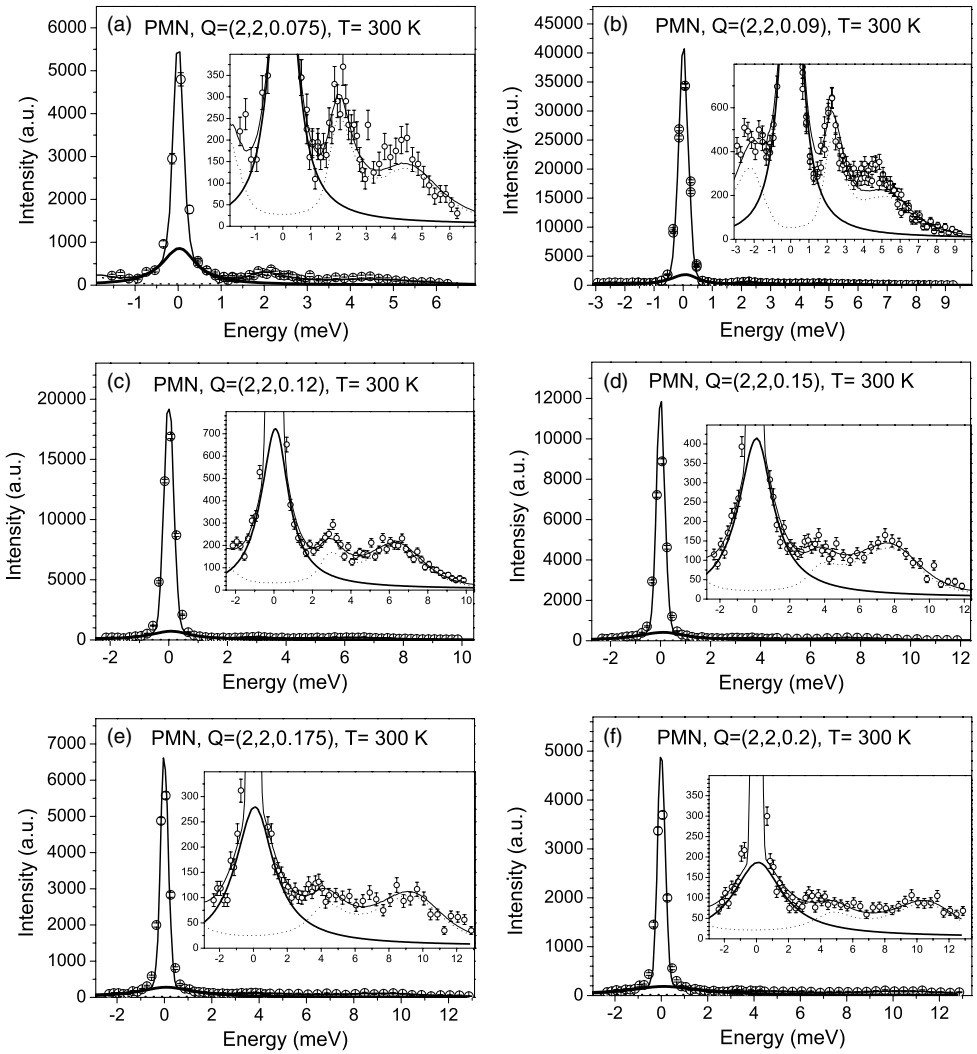

Figure 8. Observed and calculated spectra from constant-Q scans taken in the (2, 2, 0) BZ at $T = 300$ K. The contribution of the QE component is emphasized by bold solid lines. The spectrum shown in figure 8(a) was measured with configuration (iii); other spectra were measured with configuration (ii).

elastic component is also shown in figure 13 and it is consistent with a Lorentzian line shape, as suggested in equation (11). The values of the parameters characterizing the QE scattering at the temperatures of 450 and 300 K are $\xi = 7\pm2$ and 11 ± 2 Å, $\Gamma_0 = 0.3\pm0.04$ and 0.15 ± 0.03 meV, while $D_{\mathrm{QE}} = 19 \pm 2$ and 17 ± 2 meV^2 Å^2, respectively. The conclusion is that D_{QE} does not change as a function of temperature, within the precision of the measurements, but that the inverse correlation length and the damping at $q = 0$ both decrease as the temperature decreases and as illustrated for the inverse correlation length in figure 14. Below 300 K, the correlation length remains approximately temperature independent but the damping still decreases.

The component of the central peak that is resolution limited is difficult to measure because it must be distinguished from the sharp and intense Bragg reflection on the one hand and from

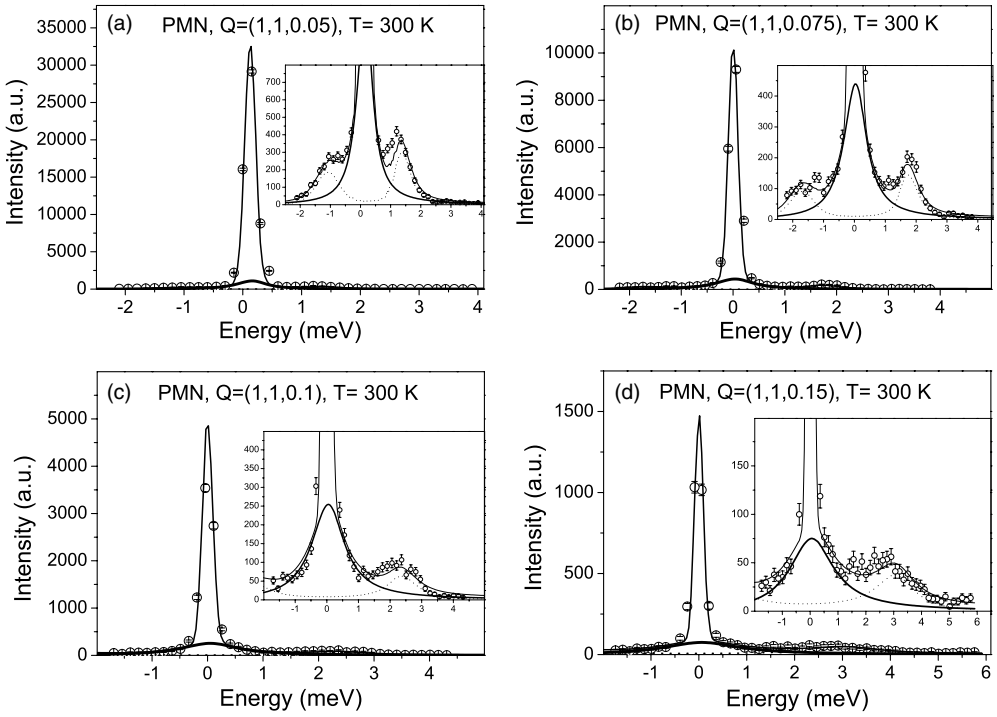

Figure 9. Observed and calculated spectra from constant-Q scans taken in the (1, 1, 0) BZ and configuration (i). The contribution of the QE component is emphasized by bold solid lines.

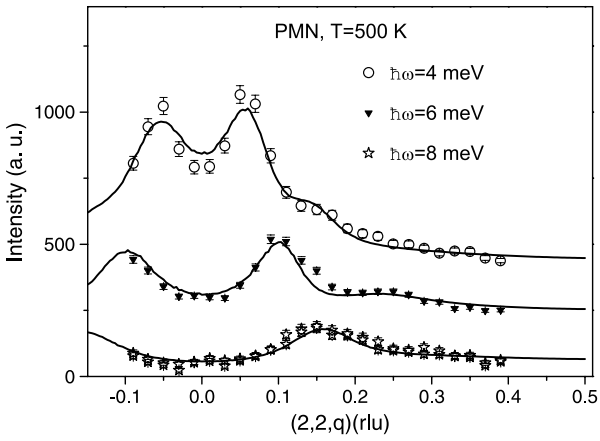

Figure 10. Constant-energy scans in PMN at $T = 500$ K. For means of comparison the scans have been shifted by 200 counts.

the incoherent scattering that is expected to vary only slowly with the wavevector. Above about 480 K the intensity of the elastic scattering is weak and away from the Bragg reflection it probably arises from the incoherent scattering. Below a temperature of 370 K the scattering rapidly increases in intensity as the sample is cooled as shown in figure 15. There appears to be some rounding possibly due to an inhomogeneous concentration distribution in the region of

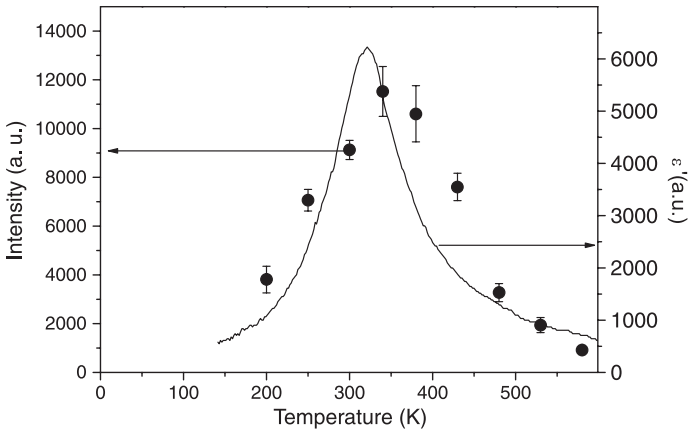

Figure 11. Temperature dependence of the susceptibility of the QE scattering in PMN measured at $\mathbf{Q} = (1, 1, 0.05)$. For comparison the real part of the dielectric permittivity of PMN at frequency 1 GHz is also shown [35].

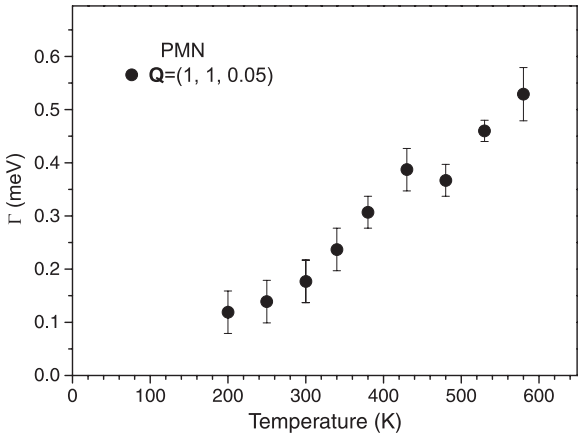

Figure 12. Temperature dependence of the damping of the QE scattering measured at $\mathbf{Q} = (1, 1, 0.05)$.

370 K. The shape of the curve is nevertheless similar to that expected from an order parameter although in wavevector it is wider than the Bragg reflection. The distribution of the intensity in wavevector is determined by $A(\mathbf{Q})$. It is known e.g. from reference [20] that the distribution of the diffuse scattering in PMN is largely perpendicular to the wavevector transfer. In figure 16 we show the measured intensity perpendicular to the (1, 1, 0) Bragg reflection at 150, 300 and 450 K. Clearly there is more diffuse scattering in the wings of the Bragg reflections at the two lower temperatures and in order to explain these results we have fitted the observations to the sum of a Bragg Gaussian, a flat background and a Lorentzian to an arbitrary power for the intermediate structure. As shown in figure 16 very reasonable descriptions were obtained when the intermediate peak was a Lorentzian to the power 1.5 while the inverse correlation function for this component slightly decreased from about 0.025(5) rlu at 300 K to 0.015(5) rlu at 150 K. We note that at any temperature, the scattering by the central peak was found to be adequately described by a Lorentzian function to a power of about 1.5 and from our analysis of

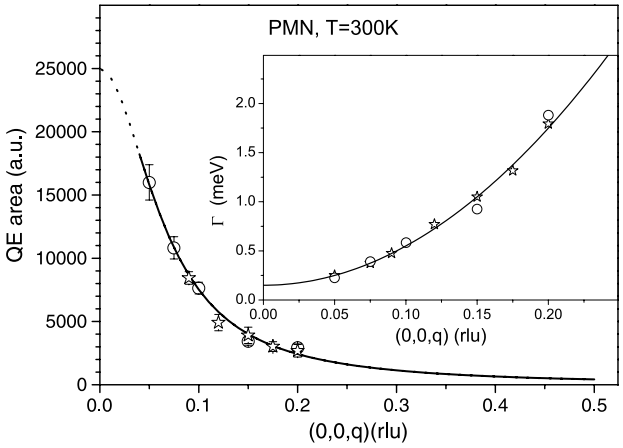

Figure 13. Wavevector dependence of the energy-integrated intensity of the QE scattering in PMN measured in (1, 1, 0) (circles) and (2, 2, 0) (stars) Brillouin zones. Intensities of the QE component in two zones are scaled by a factor ∼1.3 at $q = 0.2$ rlu. The inset shows the q dependence of the damping of the QE component; the error bars are within the symbol size.

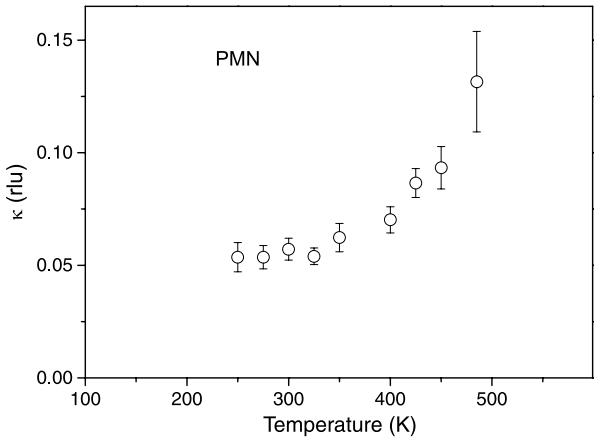

Figure 14. Temperature dependence of the inverse correlation length of the quasi-elastic scattering.

the data we conclude that the correlation length decreases above room temperature to a value of 0.04 rlu at 400 K.

4. Discussion and conclusion

We have measured the low energy phonons in the relaxor ferroelectric PMN using high resolution neutron scattering techniques. Previously [18–21] measurements were made of the neutron scattering in the (010) plane and using a more relaxed resolution function for the neutron scattering. Our results for the scattering in the $(1\bar{1}0)$ plane lead to quite a different picture and so initially we will compare and contrast our experimental results. The important phonons in PMN are the TA and lowest TO branches and we agree that there is a strong coupling between these two modes of vibration and that they can strongly interact because

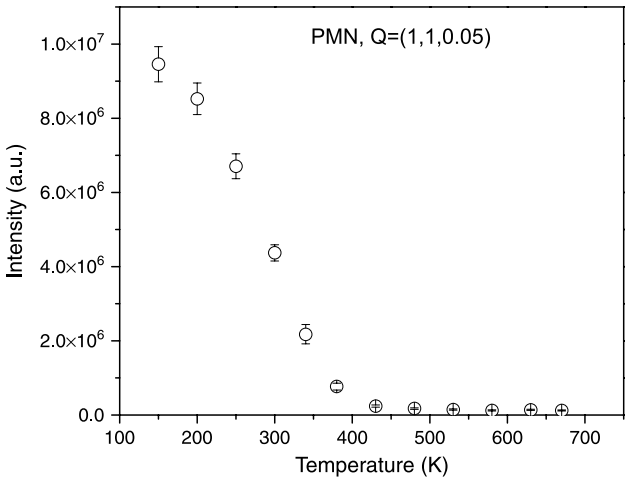

Figure 15. Temperature dependence of the intensity of the strictly elastic central peak.

they have the same symmetry. The earlier work found that above the Burns temperature 620 K the TO mode was underdamped and decreased in frequency as the temperature was decreased. Below the Burns temperature it became overdamped and the frequency could not be obtained until the sample was cooled below a temperature of 200 K when it increased in frequency and became underdamped again. Throughout this intermediate region between 200 and 620 K the TO mode exhibited the 'waterfall effect' at which the mode has an infinite slope and the wavevector is almost constant. The critical wavevector 0.2 Å^{-1} suggested that this behaviour results from the interaction of the mode with the polar nanoregions (PNR) and with the strong coupling between the mode and the TA modes. Later neutron scattering experiments [24] showed that the effect depends on the Brillouin zone and hence it is probably unlikely that it is due to the size of the PNR.

Our results differ in that throughout the region immediately below the Burns temperature we find that the inelastic scattering can be described at least at small wavevectors in terms of largely temperature independent underdamped modes particularly for the TO mode. We also did not observe a 'waterfall effect' for the TO mode. We consider that the reason for the first difference is that we used substantially better resolution than the previous work while for the second difference our observations were made in a different Brillouin zone and so our results support the conclusion of Hlinka *et al* [24] based on their results for PZN.

The high resolution of our results did enable us to distinguish two components at low energies; one was the quasi-elastic scattering and the other the central peak. We have measured the intensity scattered by the TO mode and by the QE scattering and found that the ratio differs from one Brillouin zone to another. For example, the TO mode is weak near (110) above the TA mode but the QE scattering is present. The QE scattering might arise from the TO mode through the mode coupling because at low frequencies, below the TA phonon, the TO mode would have a different eigenvector from that above the TA mode. We would then expect a different structure factor for the TO mode and the QE scattering as discussed in [20]. This effect does not however explain the difference in intensity or line shape of the scattering if the QE scattering is to be described by the interacting phonon model, outlined in the first part of section 3. We cannot however be certain that this is impossible if there is a strong frequency dependence to the self-energy of the TO mode, such as in the well known central peak problem

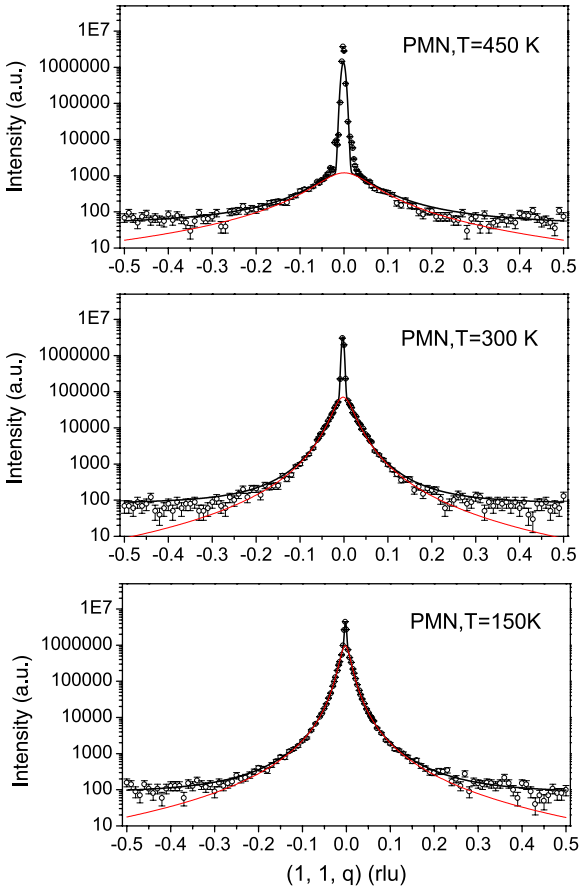

Figure 16. Temperature dependence of the intensity of the elastic scans. These measurements were performed using $k_f = 1.4$ Å^{-1} and $10'/$Å$-20'-20'-80'$ collimation.

in $SrTiO_3$ [36]. Nevertheless we shall in this paper discuss the QE scattering as though it was an independent mode of the crystal.

We observe that the quasi-elastic scattering appears below the Burns temperature T_d. Upon cooling the sample the susceptibility of the QE scattering increases rapidly and peaks around $T_m = 370$ K. Simultaneously the characteristic time of the fluctuations increases. The frequency and wavevector dependence of the scattering are strongly suggestive of a phase transition at that temperature. Thus we can conclude that below T_d we observe critical fluctuations that behave in a similar way to those of paraelectric or paramagnetic systems and one should expect a continuous phase transition when both the susceptibility and the correlation length diverge. The surprising feature is that the critical fluctuations in PMN have very low frequencies and are observed over an exceptionally wide temperature range between 200 and 600 K. Most systems undergoing a phase transition have critical fluctuations that appear much closer to the phase transition and with much higher energies. This suggests that the fluctuations in PMN involve large collections of atoms, possibly PNR, rather than individual atoms. Below T_m the susceptibility of the critical fluctuations in PMN decreases while the correlation length is approximately temperature independent, equal to 11 Å^{-1}. This situation resembles the case of an antiferromagnet in a random field.

The CP scattering is strictly elastic and so we shall assume that it is caused by short range static displacements in which case it appears as diffuse scattering and not as Bragg scattering. The theory of the phase transition in an isotropic three-dimensional ferroelectric predicts that the critical fluctuations will be perpendicular to the wavevector transfer. This scattering is then similar to that expected if the critical fluctuations of an isotropic ferroelectric were frozen in at a temperature somewhat above the phase transition. We observe that the intensity of the elastic diffuse scattering (EDF) increases strongly below $T = 370$ K, as expected for the temperature dependence of an order parameter. The FWHM of this scattering decreases below T_m indicating that static displacements are correlated over larger distances. The diffuse scattering, however, never turns into a Bragg reflection. Above T_m the diffuse scattering is very weak and disappears rapidly when approaching T_d, in agreement with the results of Hiraka *et al* [30]. Above T_m, the scattering is much weaker and it was difficult to analyse the line shape precisely, due to the presence of the strong Bragg peak. Below T_m, the line shape of the diffuse scattering is described by a Lorentzian function raised to the power of $z = 1.5$. This is similar to the behaviour of an antiferromagnetic random field system in which the profile of the scattering is, after correction for the experimental resolution, a Lorentzian squared [37, 38]. If the correction is not made the observed profile depends on the detail of the resolution function but in some cases is observed to be a Lorentzian to the power of about 1.5. This onset of the EDF scattering in PMN is very suggestive of a random field transition at 370 K at which the ferroelectric critical scattering becomes pinned by the random field associated with the atomic disorder or PNR.

It was suggested that the relaxors might be examples of random field transitions in [29]. However, a system with continuous symmetry is not expected to have a transition in the presence of a random field. Nevertheless PMN and other relaxors are cubic materials rather than being isotropic and the cubic symmetry breaks the continuous symmetry and allows for a random field transition. Most of the experimental work on random fields has been on random antiferromagnets in a uniform field which then generates a staggered antiferromagnetic field [37, 38]. The experimental results then show that it is possible to reach a number of metastable states when the sample is cooled in a field. In the case of relaxors there has been little theoretical work on developing a random field theory and in particular on the form of the transition in a cubic material. We suggest that as the sample is cooled the atomic disorder gives rise to dynamic clusters of PNR, as occurs in PMN below the Burns temperature of 620 K. These do not order because the system is effectively isotropic at elevated temperature and fluctuations prevent the establishing of static order. At a temperature of about 370 K anisotropy starts to play a role and there is a crossover to a cubic phase as opposed to an isotropic phase. The system then orders into a metastable random field phase that is stable down to the lowest temperature. The crystal reaches a uniform ferroelectric state if a large field is applied below a temperature of 210 K.

We are planning further experiments both to study the detailed shape of the ordering and to discover whether we can observe any crossover from isotopic to cubic symmetry as well as to study the QE scattering and the CP scattering in different Brillouin zones.

Acknowledgments

This work was performed at the spallation neutron source SINQ, Paul Scherrer Institut, Villigen (Switzerland), and was partially supported by RFBR grant 05-02-17822.

References

[1] Smolenskii G A, Bokov V A, Isupov V A, Krainik N N, Pasynkov R E and Sokolov A I 1984 *Ferroelectrics and Related Materials* (New York: Gordon and Breach)

[2] Cross L E 1987 *Ferroelectrics* **76** 241
[3] Westphal V, Kleemann W and Glinchuk M D 1992 *Phys. Rev. Lett.* **68** 847
[4] Viehland D, Jang S J, Cross L E and Wuttig M 1992 *Phys. Rev.* B **46** 8003
[5] Blinc R, Dolinsek J, Gregorovic A, Zalar B, Filipic C, Kutnjak Z, Levstik A and Pirc R 1999 *Phys. Rev. Lett.* **83** 424
[6] de Mathan N, Husson E, Calvarin G, Gavarri J R, Hewat A R and Morell A 1991 *J. Phys.: Condens. Matter* **3** 8159
[7] Schmidt G, Arndt H, Voncieminski J, Petzsche T, Voigt H and Krainik N 1980 *Krist. Tech.* **15** 1415
[8] Burns G and Scott B A 1973 *Solid State Commun.* **13** 423
[9] Lushnikov S G and Prokhorova S D 1989 *Ferroelectrics* **90** 187
[10] Laiho R, Lushnikov S G and Siny I G 1992 *Ferroelectrics* **125** 493
[11] Siny I G, Lushnikov S G, Katiyar R S and Rogacheva E A 1997 *Phys. Rev.* B **56** 7962
[12] Siny I G, Lushnikov S G, Kariyar R S and Schmidt V H 1999 *Ferroelectrics* **226** 191
[13] Svitelskiy O, Toulouse J, Yong G and Ye Z G 2003 *Phys. Rev.* B **68** 104107
[14] Naberezhnov A A, Vakhrushev S B, Dorner B, Strauch D and Moudden H 1999 *Eur. Phys. J.* B **11** 13
[15] Gehring P M, Park S E and Shirane G 2000 *Phys. Rev. Lett.* **84** 5216
[16] Gehring P M, Vakhrushev S B and Shirane G 2000 *Fundamental Physics of Ferroelectrics 2000* vol 535, ed R E Cohen (Melville, NY: American Institute of Physics) p 314
[17] Gehring P M, Park S E and Shirane G 2001 *Phys. Rev.* B **63** 224109
[18] Gehring P M, Wakimoto S, Ye Z G and Shirane G 2001 *Phys. Rev. Lett.* **87** 277601
[19] Wakimoto S, Stock C, Birgeneau R J, Ye Z G, Chen W, Buyers W J L, Gehring P M and Shirane G 2002 *Phys. Rev.* B **65** 172105
[20] Hirota K, Ye Z G, Wakimoto S, Gehring P M and Shirane G 2002 *Phys. Rev.* B **65** 104105
[21] Wakimoto S, Stock C, Ye Z G, Chen W, Gehring P M and Shirane G 2002 *Phys. Rev.* B **66** 224102
[22] Vakhrushev S B and Shapiro S M 2002 *Phys. Rev.* B **66** 214101
[23] Gvasaliya S N, Roessli B and Lushnikov S G 2003 *Europhys. Lett.* **63** 303
[24] Hlinka J, Kamba S, Petzelt J, Kulda J, Randall C A and Zhang S J 2003 *Phys. Rev. Lett.* **91** 107602
[25] Dorner B, Ivanov A S, Vakhrushev S B, Lushnikov S G, Gvasaliya S N, Strauch D and Schmalzl K 2003 *Ferroelectrics* **282** 9
[26] Gvasaliya S N, Strauch D, Dorner B, Lushnikov S G and Vakhrushev S B 2003 *Ferroelectrics* **282** 21
[27] Gvasaliya S N, Lushnikov S G and Roessli B 2004 *Phys. Rev.* B **69** 092105
[28] Gvasaliya S N, Lushnikov S G and Roessli B 2004 *Cryst. Rep.* **49** 108
[29] Stock C, Birgeneau R J, Wakimoto S, Gardner J S, Chen W, Ye Z-G and Shirane G 2004 *Phys. Rev.* B **69** 094104
[30] Hiraka H, Lee S H, Gehring P M, Xu G and Shirane G 2004 *Phys. Rev.* B **70** 184105
[31] Coombs G J and Cowley R A 1973 *J. Phys. C: Solid State Phys.* **6** 121
[32] Bruce A D and Cowley R A 1980 *Structural Phase Transitions* (London: Taylor and Francis)
[33] Wehner R K and Steigmeier E F 1975 *RCA Rev.* **36** 70
[34] Popovichi M 1975 *Acta Crystallogr.* A **31** 507
[35] Bovtun V, Kamba S, Pashkin A, Savinov M, Samoukhina P, Petzelt J, Bykov I P and Glinchuk M D 2004 *Ferroelectrics* **298** 23
[36] Shapiro S M, Axe J D, Shirane G and Riste T 1972 *Phys. Rev.* B **6** 4332
[37] Yoshizawa H, Cowley R A, Shirane G and Birgeneau R J 1982 *Phys. Rev. Lett.* **48** 432
[38] Cowley R A, Shirane G, Yoshizawa H, Uemura Y G and Birgeneau R J 1989 *Z. Phys.* B **75** 303